Talanta 187 (2018) 379–389

Contents lists available at ScienceDirect

Talanta

journal homepage: www.elsevier.com/locate/talanta

Electrochemical genosensor based on template assisted synthesized polyaniline nanotubes for chronic myelogenous leukemia detection

Amrita Soni[a,b], Chandra Mouli Pandey[c], Shipra Solanki[a,b], R.K. Kotnala[b], Gajjala Sumana[b,*]

[a] Academy of Scientific and Innovative Research (AcSIR), CSIR-National Physical Laboratory, New Delhi 110012, India
[b] CSIR-National Physical Laboratory, New Delhi 110012, India
[c] Department of Applied Chemistry, Delhi Technological University, Delhi 110042, India

ARTICLE INFO

Keywords:
Cancer
Electrophoretic
Polyaniline nanotubes
Biosensor

ABSTRACT

This work reports a facile approach to synthesize polyaniline nanotubes (PANI-NT) by using manganese oxide as sacrificial templates. This template assisted polyaniline nanotubes (t-PANI-NT) were utilized as electrode material after deposition onto the indium tin oxide (ITO) coated glass substrates by using the electrophoretic technique. The structural, morphological and electrochemical characterizations of the t-PANI-NT show relatively better results compared to chemically synthesized PANI-NT (c-PANI-NT). Moreover, the t-PANI-NT/ITO electrode exhibits improved electron transfer coefficient ($\alpha = 0.63$) and charge transfer rate constant ($k_s = 0.05912\ s^{-1}$) in comparison to c-PANI-NT/ITO electrode ($\alpha = 0.56$ and $k_s = 0.06548\ s^{-1}$). The obtained t-PANI-NT/ITO electrodes have been further immobilized with biotinylated DNA sequence, specific to chronic myelogenous leukemia (CML) by using avidin–biotin as a cross-linking agent. Electrochemical impedance spectroscopy studies revealed that the genosensor displays linearity in wide range of target DNA concentration (10^{-6} to 10^{-16} M) with an outstanding differentiation ability and low detection limit of 10^{-16} M. The experimental results of this highly sensitive and specific genosensor with clinical samples of CML positive patients and control negative patients indicate its potential for clinical diagnostics.

1. Introduction

Nanostructured materials show several advantages, such as large surface area, high aqueous stability and the diverse conductive mechanism that lowers the interfacial impedance between the electrode and the electrolyte compared to their bulk counterpart [1,2]. Moreover to improve the performance of the nanostructured materials the control over the size and morphology at the nanoscale is very essential [3,4]. Synthesis using a pre-existing nanostructured template is one of the most effective strategies towards achieving high degree of synthetic control with respect to size, shape, composition and spatial arrangement of nanostructured materials, which usually benefits from the directing effect of the templates [5–8]. In order to synthesize ordered conducting polymers (CP) nanostructures, it is necessary to use close-packed assemblies of templates [9,10] as polymers are highly unstable at the nanometer scale. A variety of CP nanostructures have been developed, and their reversible interchange between redox states, excellent electrical conductivity, and enhanced stability make them suitable for applications in energy conversion, storage devices, sensors, actuators, and bio-devices [11,12]. Among various CP, polyaniline (PANI) has been considered as one the most studied conductive conjugated polymer due to its unique physical and chemical properties viz. high conductivity, good environmental stability, redox behavior and biocompatibility leading to many applications in gas sensing as well as in electrochromic and electrocatalytic devices [13–15]. PANI nanostructures, e.g., nanorods, nanofibers, nanospheres offer enhanced electrochemical performance by providing high interfacial area and have great potential for the development of miniaturized devices [16,17]. Moreover, it has been indicated that the tube-like structure of PANI could increase the electrode surface area and provide shorter and direct pathways for more charge transportation and ion diffusion which facilitate the electrode volume change in charge/discharge processes [18,19]. Therefore, a robust route to synthesize PANI nanotubes (PANI-NT) with well-controlled morphology and improved electrochemical performance can play a significant role for biomedical applications [20].

Chronic myeloid leukemia (CML) is a hematopoietic stem cell malignancy arises from reciprocal translocation of t(9;22) (q34;q11.2), results in a genetic recombination between the cellular ABL proto-oncogene on chromosome 9 and the breakpoint cluster region (BCR) gene

* Corresponding author.
E-mail address: sumanagajjala@gmail.com (G. Sumana).

https://doi.org/10.1016/j.talanta.2018.05.038
Received 24 February 2018; Received in revised form 7 May 2018; Accepted 8 May 2018
Available online 21 May 2018
0039-9140/

on chromosome 22 [21,22]. The BCR/ABL chimerical fusion gene on 22q11 encodes for unrestrained tyrosine kinase which causes disorderly proliferation of leukocytes leading to blocking of apoptosis, genome instability and enlargement of the spleen, liver, and other organs, which plays a vital role in the pathogenesis of CML [23,24]. Currently, several useful and efficient clinical diagnostic techniques have been applied to recognize overexpressed, rearranged BCR/ABL fusion gene included fluorescence in situ hybridization, flow cytometry and real-time quantitative reverse transcription PCR, cytogenetics and southern blot [25,26]. But due to limitations of these methods, (time consumption, poor precision, expensiveness and error-prone nature), it becomes very significant to develop a new method that requires only a few handling steps, making the point-of-care diagnostics and monitoring of CML possible at an early stage [27–29]. In this context, electrochemical DNA biosensors have been recognized as a promising solution for simple, portable, rapid, and inexpensive sequence-specific detection of genetic diseases and other biological analysis [30–32]. Various electrochemical genosensors based on PANI nanostructures have been explored that provides a distinctive molecular platform for the immobilization of DNA in which PANI nanostructures act as molecular wires by connecting DNA molecules that provide controlled bio-molecular events [33–35].

In the present work, PANI-NT has been synthesized using both chemical and template route. The synthesized PANI-NT has been electrophoretically deposited onto indium tin oxide coated glass substrates. These PANI-NT films have been utilized for the fabrication of genosensor by immobilizing probe DNA (pDNA) sequence specific to CML, identified from the BCR–ABL gene. Further, these bioelectrodes were used for detection of CML target sequence both in synthetic DNA samples and clinical samples. To the best of our knowledge, the present work is the first report on the application of template-assisted PANI-NT based electrodes as the transducer platform for detection of cancer.

2. Experimental section

2.1. Reagents and chemicals

Potassium permanganate ($KMnO_4$), potassium dichromate ($K_2Cr_2O_7$), hydrochloric acid (HCl), avidin, 1-Ethyl-3-(3-dimethylaminopropyl)carbodiimide (EDC), N-Hydroxy succinimide (NHS), ethylene diamine tetra acetic acid (EDTA), potassium monohydrogen phosphate, potassium dihydrogen phosphate, camphor sulfonic acid (CSA), ammonium persulfate (APS), Aniline ($C_6H_5NH_2$) was distilled prior to polymerization. Indium–tin oxide (ITO) coated glass sheets with resistivity 30 Ω have been utilized. All other chemicals were of analytical grade and used without purification. For the preparation of aqueous solutions, deionized water (resistance 18.2 MΩ cm) was used. CML-specific oligonucleotide probe sequences (22 bases; UID no. 12859844) correspond specifically to P210 kDa BCR–ABL gene of Philadelphia chromosome [31], complementary, noncomplementary, one base-mismatch, two base-mismatch target sequences and all other reagents and solvents have been procured from Sigma-Aldrich Milwaukee, WI. DNA sequences used for the studies are as follows:

Probe DNA: biotin-5′-TGTCCACAGCATTCCGCTGACC-3′
Complementary DNA: 5′-GGTCAGCGGAATGCTGTGGACA-3′
One-base mismatch DNA: 5′-GCTCAGCGGAATGCTGTGGACA- 3′
Two-base mismatch DNA: 5′-GCTCAGCGCAATGCTGTGGACA-3′
Non-complementary DNA: 5′-TACTCGCAATAACGTGATCTCC-3′.

2.2. Processing of clinical samples

RNA from the blood samples of CML positive and negative patients was extracted by using QIAamp RNA blood mini-kit (Qiagen). Leukocytes were removed from lysed blood by selective erythrocyte lysis followed by repetitive homogenization and washing. Afterwards, high-capacity cDNA reverse transcription kit (Applied Biosystems) have been utilized for the reverse-transcription of separated RNA to complementary DNA (cDNA). The extracted cDNA was diluted 10 times in TE buffer and boiled in a water bath for about 5 min and then chilled in an ice bath followed by centrifugation at 12,000 rpm for about 10 min to get denatured single-stranded DNA. The aqueous layer of sample containing DNA was subjected to sonication at 24 kHz frequency for 15 min to break the long DNA strands into smaller fragments.

2.3. Apparatus and measurements

The structural and morphological characterizations of manganese oxide nanotubes (MnO_2 NT), PANI-MnO_2 nanotubes and PANI-NT have been investigated using transmission electron microscope (TEM, Hitachi Model, H-800) and scanning electron microscope (SEM, JEOLJSM-6700F, 10 kV). For elemental analysis of the materials synthesized, SEM equipped with an Energy Dispersive X-ray spectroscopy (INCA energy 250 EDX) analyzer has been used. X-ray diffraction (XRD, Rigaku Miniflex X-ray diffractometer) patterns were recorded in the 2θ range with a scan speed of 2°/min using Cu Kα radiation (λ = 0.1542 nm). Electronic conductivity was measured on compacted pellets using two probe conductivity method. Fourier Transform Infrared (FT-IR) spectroscopic investigations were performed using Perkin-Elmer spectrometer (model Spectrum BX) at 25 °C. Dynamic light scattering (DLS) measurements were performed at 25 °C with a Zetasizer Nano-ZS90 (Malvern Instruments) at a scattering angle of 90° to determine the zeta potential value of synthesized nanotubes. Contact angle (CA) investigations have been recorded using contact angle meter (Data Physics OCA15EC). Electrochemical measurements have been carried out on an Autolab potentiostat/galvanostat (Eco Chemie, Utrecht, The Netherlands) using a standard three-electrode cell system with PANI-MnO_2/ITO or PANI-NT/ITO as working electrode, Pt as an auxiliary electrode and Ag/AgCl as a reference electrode in Phosphate-buffered saline (PBS, 100 mM, pH 7.0, 0.9% NaCl) containing 5 mM of $[Fe(CN)_6]^{3-/4-}$.

2.4. Synthesis of MnO_2 nanotubes

MnO_2 NT were synthesized using earlier stated method with slight modifications [4]. In brief, 2.5 ml of concentrated HCl (37%) was added to 0.66 g of $KMnO_4$ dissolved in 75 ml of deionized water, and the solution was stirred for 15 min at room temperature. The solution was then transferred to a Teflon-lined stainless steel autoclave and was kept at a temperature of 140 °C in an electrical oven for 18 h [5]. After that, the obtained product was washed with DI water and ethanol several times till the pH value reaches to 7.0. The material was then dried in vacuum oven at 80 °C for 30 h.

2.5. Synthesis of PANI-NT by using templates

PANI-NT have been synthesized using MnO_2 as the sacrificial templates (t-PANI-NT) (Fig. 1(A)). For the synthesis, 500 mg of MnO_2 NT were dissolved in 50 ml of DI water with stirring for 15 min and further the solution was sonicated for 45 min [4]. Subsequently, 1 M HCl, 400 µl of aniline and 0.45 gm of $K_2Cr_2O_7$ was added to the solution with continuous stirring for 8 h [11], and then the mixture was allowed to stand overnight. The obtained product was collected and washed with ethanol and distilled water several times to remove the template (MnO_2 NT). The synthesized material was vacuum dried at 50 °C for 12 h. To delineate the reaction mechanism and to study the characteristics of PANI-MnO_2 NT composite for sensing applications, the material has been synthesized using the similar method at reduced reaction time interval. The products were washed carefully at mild conditions and dried at room temperature for 24 h.

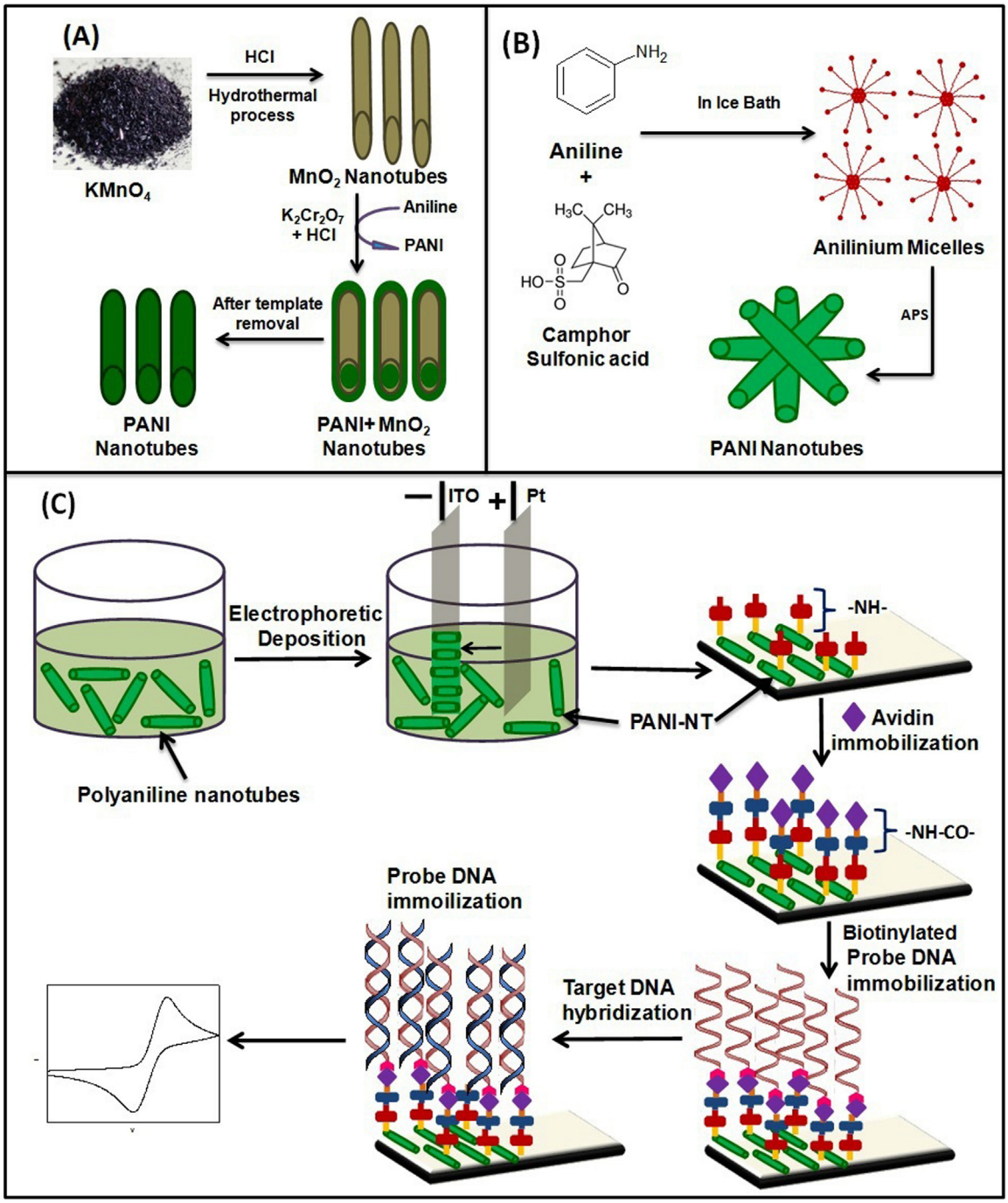

Fig. 1. Schematic illustration for the preparation of (A) PANI-NT by using MnO_2 nanotubes as reactive oxidative templates. (B) PANI-NT without using templates (C) Electrophoretic deposition of PANI-NT on ITO electrode and fabrication of pDNA/PANI-NT/ITO bioelectrode.

2.6. Synthesis of PANI-NT without using templates

Fig. 1(B) illustrates the preparation of the PANI-NT without using a template (c-PANI-NT) by chemical route [36]. In brief, 0.1 M of aniline was added to a pre-ice cooled solution of CSA (0.4 M) in 20 ml of DI water till the solution become transparent. The solution was cooled down in an ice bath, and 2 M cold aqueous solution of APS was added to the solution for oxidative polymerization [37]. The mixture was allowed to stand overnight in an ice bath. The precipitates were filtered and washed with distilled water and methanol several times and were dried in vacuum oven for 24 h at room temperature.

2.7. Electrophoretic deposition of PANI-NT and PANI-MnO_2 NT

Electrophoretic deposition (EPD) was carried out using a two electrode system, where ITO electrode was used as a cathode and thin platinum foil as an anode (Fig. 1(C)). For the deposition of t-PANI-NT onto ITO electrodes, 10 mg of t-PANI-NT was dispersed in 10 ml of ethanol and 20 V of voltage for 45 s was applied. Similarly, the deposition of c-PANI-NT on to ITO electrode was done at 100 V for 60 s by taking c-PANI-NT in a solution of 9.9 ml of acetonitrile and 100 µl of formic acid [36]. 10 mg of PANI-MnO_2 NT was dissolved in a solvent mixture of ethanol and water (1:1) and films of PANI-MnO_2 were deposited on ITO electrodes under the optimum conditions of 30 V for 60 s. The conditions were different for the two materials, due to the

variation in oxidant and dopant ($K_2Cr_2O_7$ and HCl for t-PANI-NT and APS and CSA for c-PANI-NT respectively) used for synthesizing the nanotubes, which further affect the solubility as well as depositing conditions of the material synthesized.

2.8. Fabrication of bioelectrodes for CML detection

For the fabrication of bioelectrodes, pDNA (22 base pairs) has been immobilized on the t-PANI-NT/ITO electrodes using avidin-biotin linkage. For this purpose, 20 µl of avidin was immobilized (2 h) on the t-PANI-NT/ITO platform by using EDC (0.2 M) and NHS (0.4 M) at 25 °C [38]. Subsequently, avidin-t-PANI-NT/ITO electrode was washed and incubated with biotinylated pDNA (20 µl, 1.0 mM) for 6 h in a humid chamber at 25 °C. These bioelectrodes were washed with Tris-HCl (10 mM) and EDTA (1 mM) buffer solution (TE, pH 8.0) several times to remove any unbound pDNA from the electrode surface. The fabricated pDNA/t-PANI-NT/ITO bioelectrodes were further utilized for the hybridization studies by incubating it with the target DNA sequences for 20 min in a humid chamber at 25 °C (Fig. 1(C)).

3. Results and discussion

3.1. Microscopic analysis of nanotubes

The TEM studies have been conducted to confirm the size and structure of the synthesized nanotubes. Fig. 2(A) illustrates the TEM image of MnO_2 NT synthesized using hydrothermal process, having a diameter in the range of 40–50 nm (inset of Fig. 2(A), showing MnO_2 NT with a diameter of 42 nm). MnO_2 NT exhibit smooth surface and are uniformly dispersed without formation of domains due to aggregation, which is confirmed by high-resolution transmission electron (HRTEM) microscopy image (Fig. 2(B)) of MnO_2-NT. The TEM image of c-PANI-NT (Fig. 2(C)) shows tubular structures with a diameter ranging from 90 nm to 130 nm (Fig. 2(D)), and along with nanotubes, nanofibers can also be seen in the image (Fig. 2(C)). The TEM images of PANI-MnO_2 (Fig. 3(A) and (B)) were recorded to analyze the growth process of PANI-NT on the surface of MnO_2 NT, in which, MnO_2 acts as template and oxidant or reducing agent at the same time. In Fig. 3(A), multiple layers of PANI wrapped around the surface of MnO_2 NT results in the formation of PANI-MnO_2 NT with increased diameter in the range 80–120 nm as compared to the MnO_2 NT. In Fig. 3(B), the TEM image of PANI-MnO_2 NT at higher magnification clearly reveals the coating of PANI on MnO_2 and presence of MnO_2 NT in the center can also be observed. Further, TEM studies reveal that with an increase in the reaction time the gradual growth of PANI-NT (Fig. 3(C) and (D)) and degradation of the MnO_2 template can be observed which leads to the formation of the tube-like structures of PANI (Fig. 3(C)). However, it can be seen that the t-PANI-NT exhibit the inner diameter in the range of 40–50 nm (Fig. 3(D)) which is comparable to the diameter of MnO_2 NT (Fig. 2(A)) with a wall thickness of about 14 nm. The dark areas (irregular projections) seen in Fig. 3(C) is may be due to multiple layers formed or folding of the edges of the t-PANI-NT as they are flexible and can be easily intertwined. It has been observed that t-PANI-NT are well dispersed and exhibited perfectly tubular structures (hollow) with open-ended tips (Fig. 3(C)) as compared with c-PANI-NT (Fig. 2(C)). This may be due to absence of directing effect provided by template, which also acts as driving force for the uniform synthesis of PANI-NT and without which the random accumulation of the PANI molecules will take place. Moreover, it is well known that the hydrogen bonding between the CP plays a very significant role in the development of uniform nanostructures, and disruption of which can cause formation of irregular shape of PANI-NT and further reduces the electrochemical performance of the material [16].

3.2. Characterization of PANI-NT and PANI-MnO_2 NT

Fig. 4(A) shows the XRD pattern of the MnO_2 NT. All the diffraction peaks indexed to tetragonal phase of α-MnO_2 (JCDPS No. 721982),

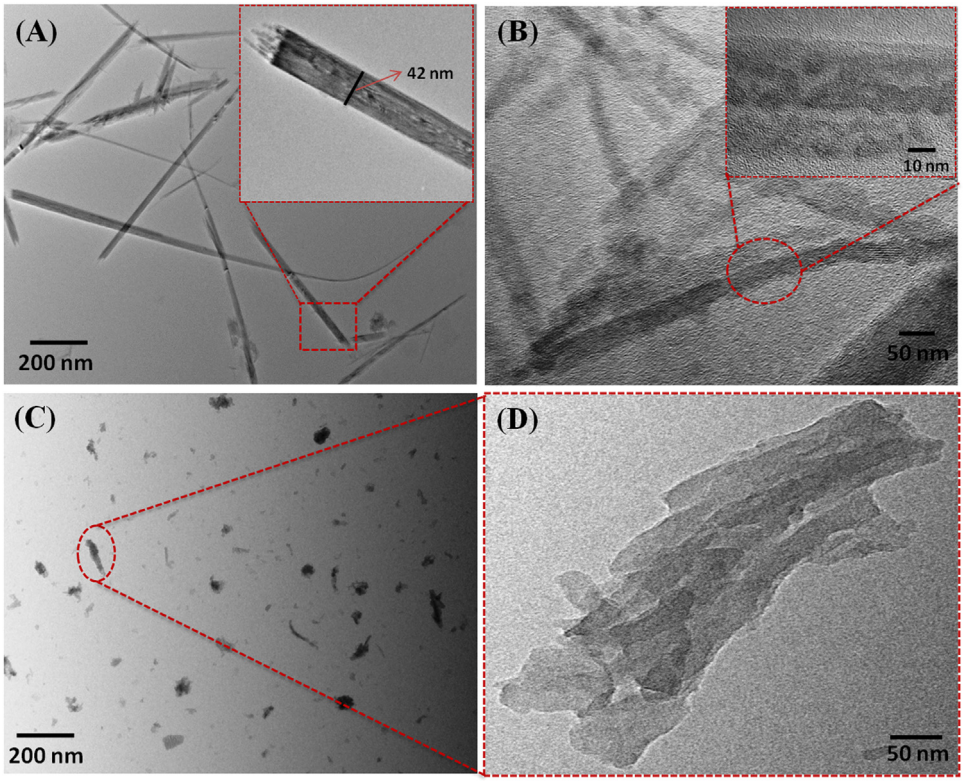

Fig. 2. (A) TEM image of MnO_2 NT (inset representing the diameter of nanotubes) (B) HR-TEM image of MnO_2 NT. TEM images of c-PANI-NT (C) at lower magnification (D) at higher magnification.

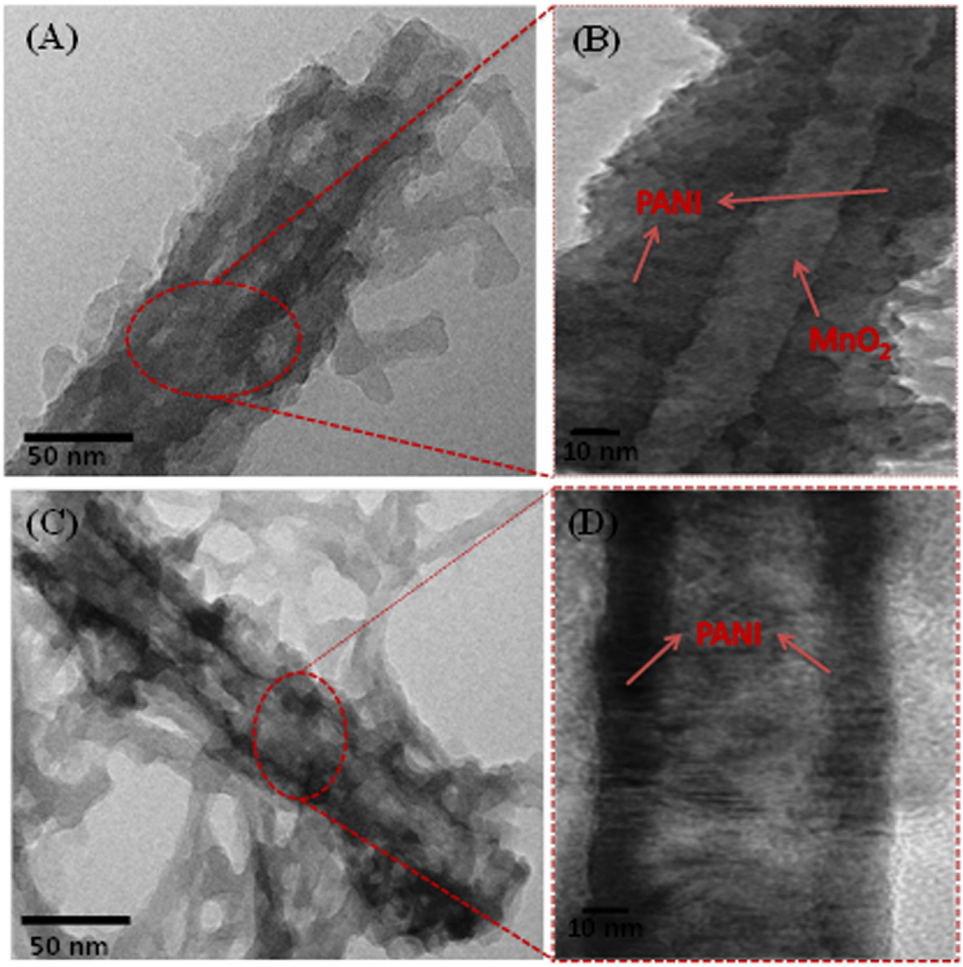

Fig. 3. TEM images of PANI-MnO_2 NT (A) at lower magnification (B) at higher magnification. TEM images of t-PANI-NT (C) at lower magnification (D) at higher magnification.

which reveals the crystalline behavior of the MnO_2 NT. After polymerization of aniline monomer, a layer of PANI has been formed on the MnO_2 NT (confirmed by the TEM image of PANI-MnO_2 (Fig. 3(A))), due to which the broadening of the peaks at $2\theta = 20.7^{\circ}$ and 26.3° can be observed, (Fig. 4(B)) representing the amorphous nature of the PANI-MnO_2 NT due to presence of PANI [39]. However, the peak at 20.7° disappears due to complete removal of the MnO_2 template, and only a single broad peak appears at $2\theta = 26.3^{\circ}$ (Fig. 4(C)) which shows controlled growth and the periodicity parallel to the polymer chains of PANI [5]. Fig. 4(D) shows the diffraction pattern of c-PANI-NT where a broad range of peaks from $2\theta = 18.3^{\circ}$ to 29.2° was observed, which signifies the ordered structure of the polymer chains having amorphous nature of the nanotubes synthesized. The XRD results in Fig. 4(C) and (D) inferred that the crystallinity of PANI nanostructures could be changed not only by the structure of the dopants used but also by controlling the morphology of PANI nanostructures [11].

The electrical conductivities of the synthesized PANI-MnO_2 NT, t-PANI-NT and c-PANI-NT, were carried out using two probe method at room temperature. The conductivity value of t-PANI-NT (4.16×10^{-2} S/cm) shows an improvement of about two orders of magnitude compared to the conductivity of PANI-MnO_2 NT (1.72×10^{-6} S/cm), which is probably due to the non-conducting nature of MnO_2, that provides more resistance to charge flow [5]. Moreover, the conductivity value of t-PANI-NT was also found higher as compared to c-PANI-NT (2.1×10^{-3} S/cm). This increased value indicates that the conductivity of the PANI nanostructures not only depends on the strength of the doping agent used and ionic bonding with the imine nitrogen but also on the synthesis route used and morphology of nanostructures, which further offer low potential energy to electron transfer and provide high electrochemical stability [40].

EDX studies were conducted to distinguish the chemical composition of material synthesized. EDX spectrum in the Fig. S1(A) displays the peaks corresponding to Mn and O, confirming the presence of MnO_2. However, the EDAX spectrum of PANI-MnO_2 (Fig. S1(B)) shows additional peaks of C and N, which correspond to the polymerization of the aniline on the MnO_2 templates (the Cl peak is present due to doping by HCl). Whereas, no Mn peaks were observed after the removal of Mn (Fig. S1(C)), indicating complete removal of the MnO_2 templates and the successful preparation of the t-PANI-NT. The inset of the each Fig. S1(A)–(C) describes the % weight of the each element present in the products.

The zeta potential values of the synthesized PANI-MnO_2, t-PANI-NT and c-PANI-NT have been measured via dynamic light scattering. Smoluchowski method was used to determine the total charge on the surface of prepared nanostructures (Fig. S2) [41]. The PANI-MnO_2 NT exhibited a zeta potential value of 13.4 mV (Fig. S2(A)) whereas, t-PANI-NT had a value of 31.6 mV (Fig. S2(B)) and c-PANI-NT had 28.5 mV (Fig. S2(C)) of charge on the surface. The high zeta potential of t-PANI-NT indicates stability of these nanostructures, which is the required characteristic for the electrophoretic deposition.

3.3. Morphological studies of prepared electrodes and bioelectrode

The surface morphological studies of the synthesized MnO_2 NT, t-

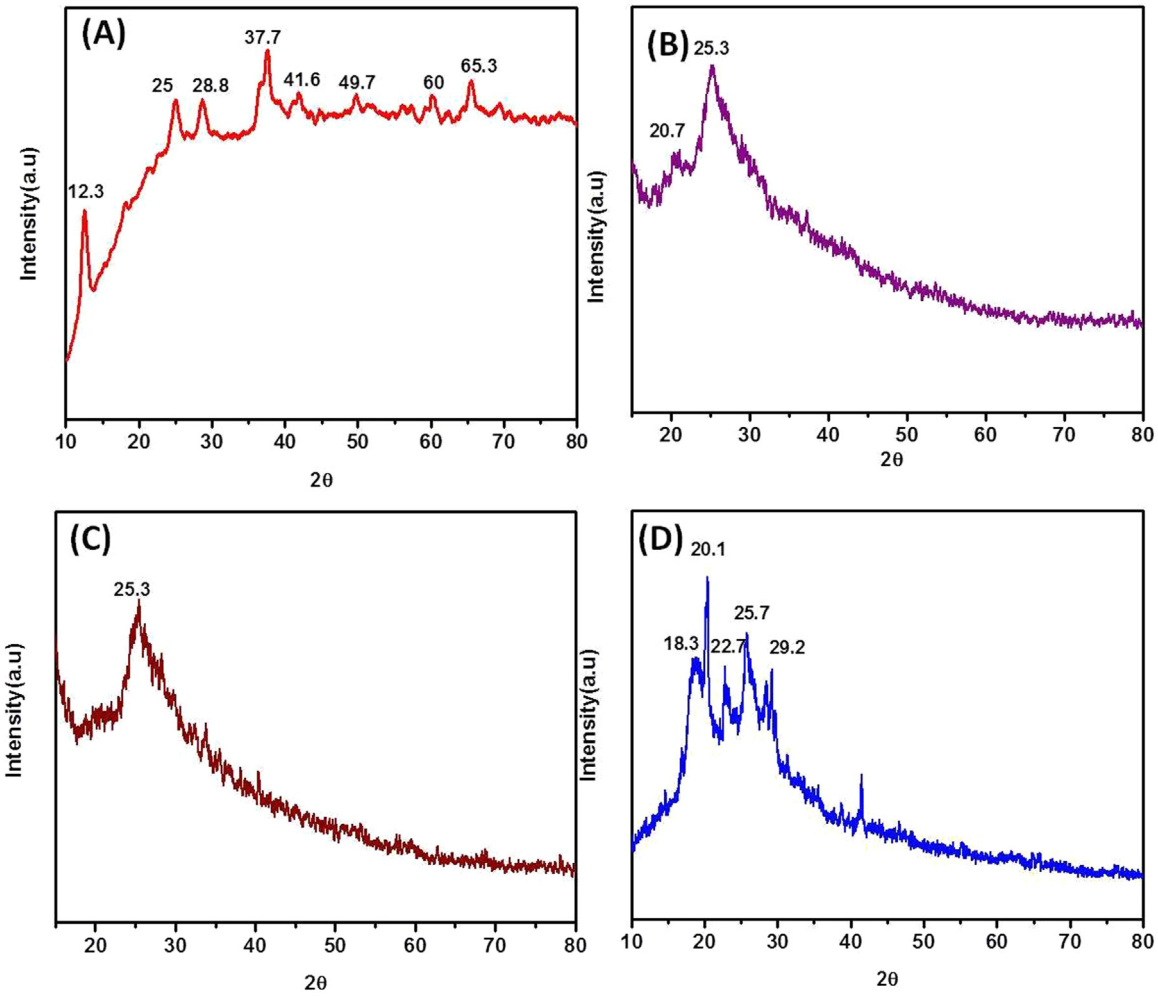

Fig. 4. X-ray diffraction patterns of (a) MnO_2 NT (b) PANI-MnO_2 NT (c) t-PANI-NT (d) c-PANI-NT.

PANI-NT/ITO electrode and c-PANI-NT/ITO electrode and pDNA/t-PANI-NT/ITO bioelectrode have been investigated using SEM. Fig. 5(A) demonstrate the SEM image of MnO_2 NT synthesized by hydrothermal reaction. The SEM image of c-PANI-NT/ITO electrode (Figs. 5(B) and S3(A)) indicates the agglomeration of the nanotubes that leads to the formation of clusters on the surface (inset Fig. 5(B)). Figs. 5(C) and S3(B) shows the morphology of t-PANI-NT/ITO electrode, where the nanotubes formed are in isolation without any agglomeration, maintaining their nanotubular structure and also exhibit the dense particle distribution. After incubation of the pDNA on t-PANI-NT/ITO electrode (Fig. 5(D)) the change in the morphology can be correlated to the immobilization of pDNA. The uniform morphology is due to even distribution of t-PANI-NT on the surface of ITO electrode that may provide a favorable environment for the immobilization of pDNA in an oriented manner [42,43].

3.4. FT-IR spectroscopic and contact angle measurements

Fig. S4 shows the FT-IR spectrum of the PANI-MnO_2/ITO, t-PANI-NT/ITO, c-PANI-NT/ITO electrodes and pDNA/PANI-NT/ITO bioelectrode. In the FT-IR spectrum of PANI-MnO_2/ITO electrode (Fig. S4(A)), the peaks at 524 and 722 cm^{-1} correspond to Mn–O stretching vibrations which are not present in the FT-IR spectrum of t-PANI-NT/ITO electrode (Fig. S4(B)) which clearly reveals the absence of MnO_2 in t-PANI-NT. Peak centered at 1364 cm^{-1} (Fig. S4(A)) is due to O–H stretching vibrations of Mn atom and vibrational peaks centered at 1581 and 1467 cm^{-1} are attributed to the stretching peaks of quinone and benzene ring deformations of PANI respectively. Whereas the FT-IR spectrum of t-PANI-NT (Fig. S4(B)) shows characteristic peaks of quinoid and benzenoid vibrations, that get shifted due to the removal of the template and are at 1582 and 1494 cm^{-1} respectively. Moreover, IR spectrum of t-PANI-NT shows (Fig. S4(B)) peak at 1295 cm^{-1} which corresponds to C–N stretching vibration of secondary aromatic amine, whether the peak at 1140 cm^{-1} corresponds to the characteristic N = Q = N stretching mode of the quinoid unit of PANI, and 801 cm^{-1} peak is assigned to C–H out-of-plane bending of 1,4 disubstituted benzene. However, in FT-IR spectrum of PANI-MnO_2/ITO electrode (Fig. S4(A)) very weak signals corresponding to the vibrational modes of PANI can be observed which are due to the presence of MnO_2 template [44]. The FT-IR spectrum of c-PANI-NT/ITO electrode (Fig. S4(C)), shows peaks at 1571 and 1495 cm^{-1} that correspond to stretching vibrations of the quinoid and benzenoid ring respectively. The band observed at 1290 cm^{-1} corresponds to C–N stretching vibration with aromatic conjugation and peak at 1160 cm^{-1} attributed to aromatic C–H in-plane bending while the peak at 830 cm^{-1} is due to bending vibrations of C-H bond in 1, 4 disubstituted benzene. The bands at 1034 and 595 cm^{-1} are assigned to absorption of -SO_3 H group indicating doping of PANI with CSA [13]. Fig. S4(D) shows the FT-IR spectrum of pDNA/t- PANI-NT/ITO bioelectrode, where the absorption bands at 1068 and 1231 cm^{-1} are due to the asymmetric stretching of P–O–C vibration and stretching vibration of P = O of the phosphoric acid group respectively. Whereas, the stretching vibration of C = C in the purine and pyrimidine attributed to carbonyl group was observed at 1550 and 1603 cm^{-1} respectively.

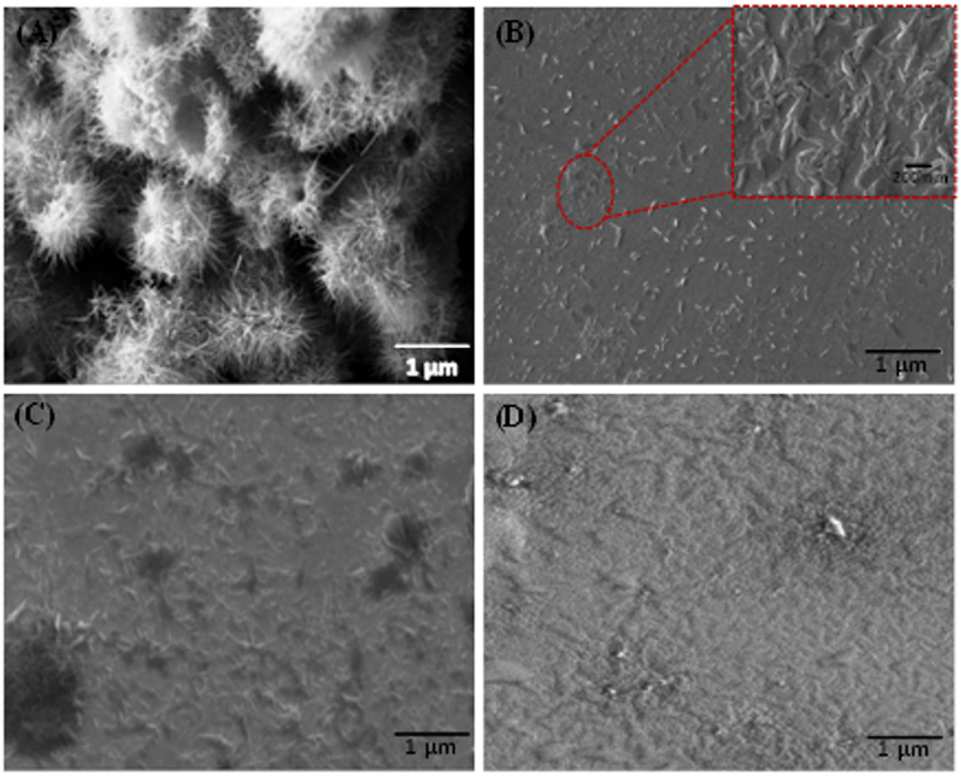

Fig. 5. SEM images of (A) MnO_2 NT (B) c-PANI-NT/ITO electrode (inset representing the image at higher magnification) (C) t-PANI-NT/ITO electrode (D) pDNA/t-PANI-NT/ITO bioelectrode.

Contact angle (CA) studies have been carried out using the sessile drop method to investigate the hydrophilicity/hydrophobicity of the electrodes and bioelectrodes. CA of pristine ITO electrode was measured to be 69.8° (Fig. S5(A)), which increases to 84.2° for PANI-MnO_2/ITO electrode (Fig. S5(B)). This increase is may be due to the introduction of hydrophobic groups on the surface of ITO electrode. The value CA for c-PANI-NT/ITO electrode was found to be 59.1° (Fig. S5(C)) and for t-PANI-NT/ITO electrode was 30.3° (Fig. S5(D)). The subsequent decrease in the value of CA can be directly related to more availability of hydrophilic functional groups (–NH_2) on the surface of the electrodes. The decrease in CA to 13.2° after the immobilization of pDNA (Fig. S5(E)) on t-PANI-NT/ITO electrode surface is due to the presence of hydrophilic negatively charged phosphodiester backbone of pDNA, which in turn can be related to incubation of pDNA on the electrode surface [42].

3.5. Electrochemical characterizations

To examine the electro-active behavior of PANI-MnO_2/ITO electrode, t-PANI-NT/ITO electrode, c-PANI-NT/ITO electrode and pDNA/t-PANI-NT/ITO bioelectrode, electrochemical studies have been carried out in phosphate buffer saline (100 mM, pH 7.0, 0.9% NaCl) containing 5 mM of $[Fe(CN)_6]^{3-/4-}$. An increase in the cyclic voltammetry peak current was observed for t-PANI-NT/ITO electrode (1.01 mA, Fig. S6(A); curve (iv)) compared to PANI-MnO_2/ITO electrode (635.30 μA, Fig. S6(A); curve (ii)), c-PANI-NT/ITO electrode (863.23 μA, Fig. S6(A); curve (iii)) and ITO (451.28 μA, Fig. S6(A); curve (i)) electrode. The higher peak current for t-PANI-NT/ITO electrode compared to PANI-MnO_2/ITO electrode, and c-PANI-NT/ITO electrode is due to the better transportation and diffusion of electrolyte ions in the electrochemical cell. Moreover, the presence of less conducting MnO_2 core also limits the access of electrolyte to the entire composite surface. However, upon immobilization of pDNA on to t-PANI-NT/ITO electrode decrease in the value of peak current (716.26 μA, Fig. S6(B); curve (ii)) has been observed which further decreases after hybridization with the target DNA (604.00 μA, Fig. S6(B); curve (iii)). This decrease in the current is due to the presence of a long chain of DNA that slows the electron transfer across the bioelectrode.

To investigate the various kinetic parameters, the cyclic voltammograms of the PANI-MnO_2/ITO, c-PANI-NT/ITO, and t-PANI-NT/ITO electrodes (Fig. S7) were recorded as a function of scan rate (10–300 mV s^{-1}). It has been observed that by increasing scan rate, the oxidation peak gets shifted towards more positive potential and reduction peak gets shifted in the reverse direction, exhibiting a quasi-reversible process. The redox peak current values of these electrodes follow a linear relationship with respect to the square root of scan rate, indicating the existence of diffusion-controlled electrochemical reaction (inset Fig. S7(A)–(C)) [45]. Both the redox peak potential values were found to be linearly dependent on the log of the scan rate which agrees with the Laviron's theory [42].

$$E_{pa} = E^o + Xln[(1-\alpha)Fv/RTk_s] \quad (1)$$

$$E_{pc} = E^o + Yln[\alpha Fv/RTk_s] \quad (2)$$

$$lnk_s = \alpha ln(1-\alpha) + (1-\alpha)ln\alpha - ln(RT/nFv) - \alpha(1-\alpha)nF\Delta Ep/RT \quad (3)$$

The value of electron transfer coefficient (α), for n number of electrons, was measured from the slopes of straight lines plotted, 2.303RT/(1 − α)nf and −2.303RT/αnf for the anodic peak potential (E_{pa}) and cathodic peak potential (E_{pc}) versus *ln ν* respectively. The values of α and K_s for different electrodes (PANI-MNO_2/ITO, t-PANI-NT/ITO and c-PANI-NT/ITO) are represented in the Table 1. By using Randles–Sevcik equation [42]

$$Ip = (2.99 \times 10^5)\alpha^{1/2}n^{3/2}AC^{1/2}v^{1/2} \quad (4)$$

The diffusion coefficient (D) was determined by a concentration gradient of $[Fe(CN)_6]^{3-/4-}$ ions between bulk and interface. Here, C is the molar concentration of $[Fe(CN)_6]^{3-/4-}$, n is the number of transferred

Table 1
Kinetic parameters calculated for the PANI-MnO_2/ITO, t-PANI-NT/ITO and c-PANI-NT/ITO electrodes.

Name of electrode	Electron transfer coefficient, α	Charge transfer rate constant,(k_s/s^{-1})	Effective surface area,(A_{eff}/mm^2)	Diffusion coefficient, D(cm^2 s^{-1})
PANI-MnO_2/ITO	0.29	0.08396	0.497	3.01×10^{-14}
c-PANI-NT/ITO	0.56	0.06548	0.599	3.26×10^{-14}
t-PANI-NT/ITO	0.63	0.05912	0.711	4.59×10^{-14}

electrons for the redox reaction, and v is the scan rate (50 mV s^{-1}). By using the calculated diffusion coefficient, the electroactive surface area (A) of the different electrodes has been calculated using Eq. (5).

$$A = S/(2.99 \times 10^5)\alpha^{1/2}n^{3/2}CD^{1/2} \quad (5)$$

The various kinetic parameters calculated for the different electrodes have been summarized in Table 1. The enhanced kinetic parameters of t-PANI-NT/ITO electrode in comparison to PANI-MNO_2/ITO electrode are due to the restricted diffusion and transportation of the electrolyte ions as MnO_2 is present in the center and prevents the effective use of the inner surface of the PANI-NT. Moreover, the kinetic parameters of t-PANI-NT/ITO electrodes (Table 1) are also better than c-PANI-NT/ITO electrodes, which is due to more ordered arrangements of t-PANI-NT onto ITO electrode providing more surface area and improved charge transfer.

Electrochemical impedance spectroscopy (EIS) is an effective technique for studying the electronic characteristics of the electrodes before and after surface modification at electrode-solution interface. The characteristic EIS plots of the different electrodes (PANI-MNO_2/ITO,t-PANI-NT/ITO, and c-PANI-NT/ITO) are illustrated in Fig. 6(A), and an equivalent circuit (Randles model) is mentioned in the inset of Fig. 6(A). The R_{ct} is the interfacial electron-transfer resistance, C_{dl} corresponds to the double-layer capacitance, R is the ohmic resistance, and Z_w is the Warburg impedance. EIS was carried out in the frequency range 0.01–10^5 Hz, and phosphate buffer (100 mM, pH 7.0, 0.9% NaCl), $[Fe(CN)_6]^{3-/4-}$ was used as a redox marker. In the Nyquist impedance plot (Z_{re} *versus* Z_{im}), semicircle portion observed at higher frequencies represents the electron-transfer-limited process, and the lower frequency portion represents the diffusion-limited transport of the redox ions in the electrolyte to the electrode interface. Change in the diameter of the semicircle has been utilized to see the corresponding change in the electron-transfer resistance (R_{ct}) of the electrodes [46]. The R_{ct} value of the t-PANI-NT/ITO electrode (554 Ω) (Fig. 6(A); curve (i)) was lower in comparison to the c-PANI-NT/ITO electrode (670 Ω) (Fig. 6(A); curve (ii)) and the PANI-MnO_2/ITO electrode (735 Ω) (Fig. 6(A); curve (iii)). This decrease in the R_{ct} value for t-PANI-NT/ITO electrode is due to the higher conductivity value of t-PANI-NT, which facilitates the fast charge transfer capability and perfectly tube-like structures, higher protonation level of t-PANI-NT provides a more exposed surface to carryout electrochemical reactions. Further, after immobilization of probe DNA sequence on the t-PANI-NT/ITO electrode there was an increase in the R_{ct} value to 1115 Ω (Fig. 6(B); curve (ii)), suggesting the presence of negatively charged (phosphate group) pDNA on the electrode surface which repels negatively charged redox marker $[Fe(CN)_6]^{3-/4-}$. After incubating the pDNA/t-PANI-NT/ITO electrode with complementary target DNA sequence (cDNA), there was an increase in the R_{ct} value (Fig. 6(B); 3590 Ω; curve (iii)) which is may be due to the introduction of more negatively charged moieties (hybridization) onto the bioelectrode surface.

3.6. Electrochemical response studies of the bioelectrode

For sensitivity studies of the pDNA/t-PANI-NT/ITO bioelectrode, we have used EIS as a suitable investigation technique (Fig. 7(A)). It was observed that the R_{ct} value increases with increasing the cDNA concentration, indicating more hybridization reaction of pDNA with target DNA. The linear increase in the R_{ct} value is due to the increased negative charge on the bioelectrode that inhibits the electron-transfer kinetics. The analytical signal (in terms of $\Delta R_{ct} = R_{ct}c_{DNA} - R_{ct}p_{DNA}$) exhibited a linear relationship with the logarithmic value of the complementary target DNA concentration ranging from 10^{-16} to 10^{-6} M for pDNA/t-PANI-NT/ITO bioelectrode (Fig. 7(B); curve (i)) and from 10^{-13} to 10^{-6} M for pDNA/c-PANI-NT/ITO bioelectrode (Fig. 7(B); curve (ii)). The pDNA/t-PANI-NT/ITO bioelectrode exhibited linear regression coefficient (RC) of 0.9980 with standard deviations of 0.62 and for pDNA/c-PANI-NT/ITO bioelectrode the value of RC and standard deviations were found to be 0.9968 and 0.76, respectively. The imprecision of the data indicated by error bars and was found to be < 4% for pDNA/t-PANI-NT/ITO bioelectrode and < 6% for pDNA/c-PANI-NT/ITO. The analytical signal (ΔR_{ct}) is represented by following equation [47]:

$$\Delta R_{ct} = 73.030 logC + 1028.957 \quad (6)$$

The detection limit was calculated using the equation (3σ/sensitivity)[47], and the value was found to be 1×10^{-16} M (Fig. 7(B); curve (i)) for pDNA/t-PANI-NT/ITO and 1×10^{-13} M (Fig. 7(B); curve

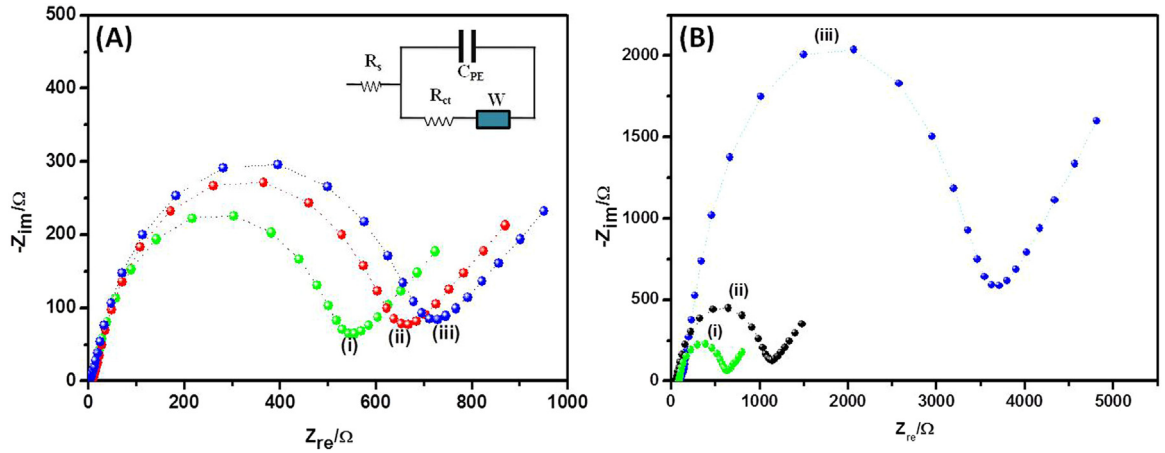

Fig. 6. Nyquist diagram for the Faradic impedance of (A) (i) t-PANI-NT/ITO electrode (ii) c-PANI-NT/ITO electrode (iii) PANI-MnO_2/ITO electrode (B) (i) t-PANI-NT/ITO electrode (ii) pDNA/t-PANI-NT/ITO bioelectrode (iii) pDNA/t-PANI-NT/ITO bioelectrode after hybridization with complementary target DNA sequence.

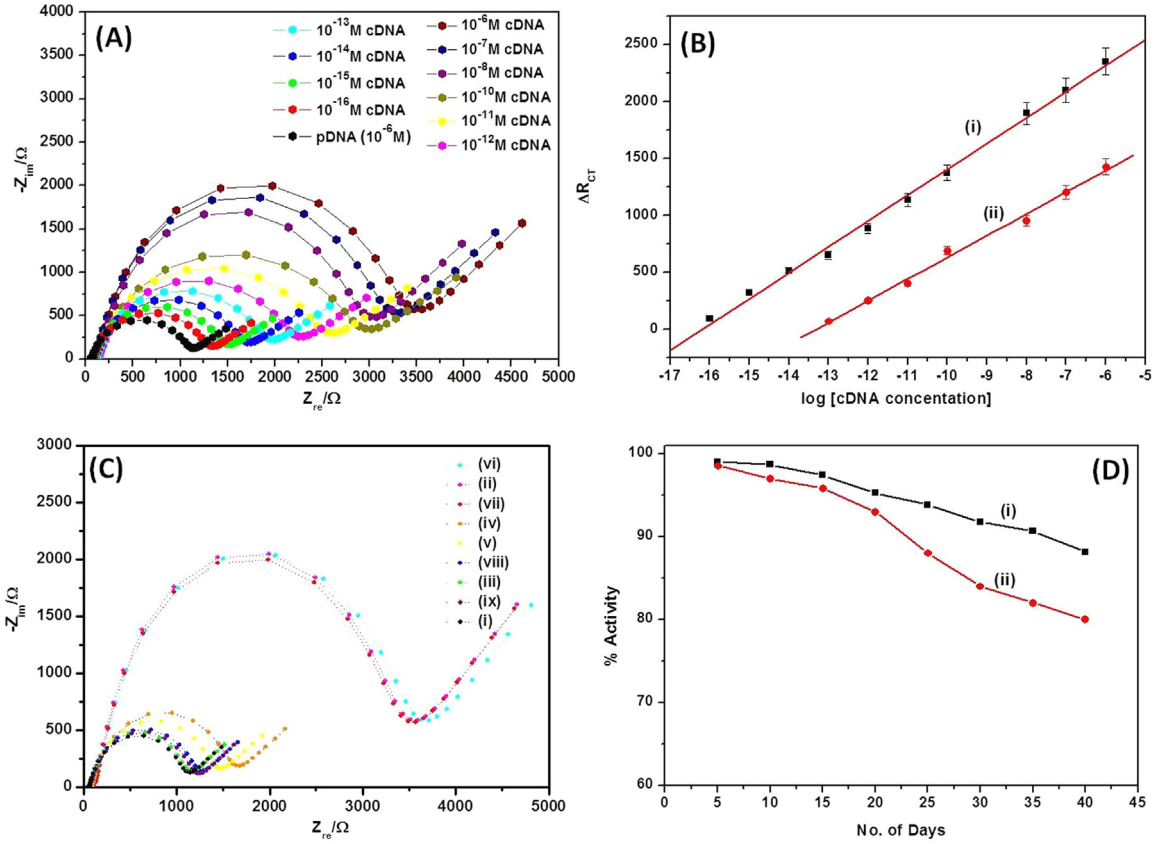

Fig. 7. (A) EIS response of pDNA/t-PANI-NT/ITO bioelectrode as a function of cDNA concentration (10^{-16} to 10^{-6} M) (B) Linearity relation curve between ΔR_{ct} and log of concentrations of cDNA for (i) pDNA/t-PANI-NT/ITO bioelectrode (ii) pDNA/c-PANI-NT/ITO bioelectrode (C) EIS response of pDNA/t-PANI-NT/ITO bioelectrode (i) with (ii) complementary (iii) non-complementary (iv) one-base mismatch (v) two base mismatch (vi) CML positive patient sample1 (vii) and sample 2 (viii) CML negative patient sample 1 (ix) and sample 2 (D) Stability of the (i) t-PANI-NT/ITO electrode and (ii) c-PANI-NT/ITO electrode after 40 days.

(ii)) for pDNA/c-PANI-NT/ITO bioelectrode, where σ is the standard deviation of the electrode without hybridization. The improved detection limit of the pDNA/t-PANI-NT/ITO bioelectrode in comparison to the pDNA/c-PANI-NT/ITO bioelectrode is due to the ordered arrangement and appropriate orientation of the pDNA onto t-PANI-NT/ITO electrode.

3.7. Selectivity and real sample analysis of bioelectrode

Selectivity studies of the prepared pDNA/t-PANI-NT/ITO bioelectrode were conducted by incubating it with different target DNA sequences (complementary, noncomplementary, one base mismatch and two base mismatch). When the pDNA/t-PANI-NT/ITO bioelectrode (Fig. 7(C); R_{ct} = 1115 Ω, curve (i)) was incubated with complementary target DNA sequence, there was a markable increase in the R_{ct} value (Fig. 7(C); 3590 Ω; curve (ii)) with respect to pDNA, which shows complete hybridization with the probe sequence. After incubation with non-complementary DNA sequence, no significant change in the R_{ct} value (Fig. 7(C); curve (iii)) was observed in comparison to the pDNA/t-PANI-NT/ITO bioelectrode indicating non-hybridization at the electrode surface due to mismatching of the DNA base pairs. However, after incubating the pDNA/t-PANI-NT/ITO bioelectrode with one base and two base mismatch DNA sequences, a slight increase in the R_{ct} value to 1664 Ω (Fig. 7(C); curve (iv)) and 1497 Ω (Fig. 7(C); curve (v)) for one base mismatch and two base mismatch respectively was obtained. This slight increase in the R_{ct} value indicates the partial hybridization of the target DNA with pDNA. This shows that the fabricated bioelectrode is even able to distinguish a single nucleotide variation during hybridization, in target DNA sequence.

3.8. Validation with clinical samples

Biosensor response studies with clinical patient samples have been recorded by measuring the change in the R_{ct} value after incubating the bioelectrode with different positive and negative patient samples of CML and are shown in Fig. 7(C). It was observed that the R_{ct} values (Fig. 7(C); curve (vi and vii)) of the CML positive patient samples are similar to the R_{ct} value of cDNA, indicating the complete hybridization however, no significant change in the R_{ct} value (Fig. 7(C); curve (viii and ix)) was seen when pDNA/t-PANI-NT/ITO bioelectrode was incubated with CML negative patient samples.

The change in the R_{ct} values for cDNA and CML positive and negative patient samples after incubating with pDNA/t-PANI-NT/ITO bioelectrode was also statistically analyzed by Analysis of Variance (ANOVA) by using Mann Whitney *t*-test for multiple comparisons (Fig. S9). Statistical significance threshold was set at 0.05 ($p < 0.05$). On hybridizing the pDNA/t-PANI-NT/ITO bioelectrode (Fig. S9(i)) with complementary target DNA the change in the R_{ct} value was found significant ($n = 3$, $p < 0.05$) (Fig. S9(ii)) in comparison to the pDNA/t-PANI-NT/ITO bioelectrode. Whereas, we did not observe a significant difference in the R_{ct} value for CML negative patient samples and in comparison to pDNA/t-PANI-NT/ITO bioelectrode ($n = 3$, $p > 0.05$) (Fig. S9(v) and (vi)). However, R_{ct} value for the CML positive patient samples were found to be statistically different, when compared with the R_{ct} value of bioelectrode ($n = 3$, $p < 0.05$) (Fig. S9(iii) and (iv)). The results indicate the validity of genosensor for detecting clinical patient samples.

Table S1 shows the comparative analysis of the results obtained from RT-PCR and biosensing assay for four different samples of both CML-positive and negative patients, having BCR-ABL transcript levels

Table 2
Comparison of the response characteristics of t-PANI-NT/ITO electrodes with other polyaniline based nanocomposites.

S. No.	Electrode	Method of immobilization	Electrochemical technique	Detection limit (M)	Detection range (M)	Hybridization time	Ref.
1.	Polyaniline nanowire deposited on GCE	EDC/NHS	SWV	1.0×10^{-15}	2×10^{-15}–8×10^{-13}	60 min	[49]
2.	BdNG-avidin-nsPANI/ITO	Biotin-avidin coupling	DPV, CV	0.5×10^{-15}	1×10^{-16}–1×10^{-6}	60 s	[38]
3.	PANI/rBi_2S_3 nanocomposite on carbon paste electrode	Covalent bonding	EIS, CV	4.37×10^{-16}	1×10^{-15}–1×10^{-11}	40 min	[50]
4.	PPy–PANi–Au nanocomposite	Covalent bonding	EIS, CV	1×10^{-13}	1×10^{-13}–1×10^{-6}	90 min	[51]
5.	Polyaniline/Pristine Graphene on GCE	Covalent bonding	EIS	0.01×10^{-12}	1×10^{-10}–1×10^{-6}	20 min	[52]
6.	t-PANI-NT/ITO	Biotin-avidin coupling	EIS, CV	1×10^{-16}	1×10^{-16}–1×10^{-6}	20 min	Present work

ranging from 0% to 85%. It was observed that the R_{ct} increases after hybridization with the PCR-amplified positive real samples, having elevated levels of transcript, whereas negligible change in the value is obtained with the negative patient samples (Fig. 7(C)). The percentage change in the R_{ct} value of the positive as well as negative patient samples in comparison to the R_{ct} value obtained for the target DNA indicates that the R_{ct} value for the positive patient samples has less percentage of variation in comparison to the target DNA while percentage of variation in R_{ct} value is more for negative patient samples (Table S1). Hence, the results obtained for the genosensor are comparable with the PCR-amplified real samples, which reveal that the present biosensing assay is suitable for the detection of BCR-ABL transcript. The comparison of response characteristics of the fabricated biosensor for CML detection have been done with other PANI based biosensors reported in the literature (Table 2), and it can be deduce that the fabricated biosensor shows better sensitivity and stability compared to other biosensors.

The potential of fabricated pDNA/t-PANI-NC/ITO bioelectrode relating to hybridization detection in human serum samples spiked with CML genomic DNA was investigated by using EIS (Fig. S8(A)). For the preparation of spiked samples, different concentrations of genomic DNA (10^{-15} M, 10^{-12} M, 10^{-8} M) in 10% human serum samples were prepared. After incubating the spiked DNA with pDNA/t-PANI-NC/ITO bioelectrode, the R_{ct} values was calculated for the different concentration. The increased values of the R_{ct} and reduced detection limit (10^{-15} M) for the serum samples in comparison to the R_{ct} values and detection limit (10^{-16} M) obtained for synthetic DNA samples is due to interference produced by different metabolites present in serum samples [48]. The curve obtained between the logarithmic values of various concentrations of the genomic DNA, spiked into diluted samples of human serum exhibited linear relationship with respect to their corresponding R_{ct} values. The results indicate that the recoveries were 93.6% (10^{-15} M), 94.8% (10^{-12} M) and 98.2% (10^{-8} M), suggesting the good accuracy of the developed method.

3.9. Reusability, reproducibility and stability of pDNA/t-PANI-NT/ITO

Regeneration studies of the prepared bioelectrodes were conducted by immersing it into the buffer solution containing 10 mM Tris-HCl and 1 mM of EDTA (pH 8.0) at 100 °C for 5 min. Then the fabricated bioelectrode was cooled down in the ice bath for ~ 30 min, the procedure removes the hybridized DNA *via* thermal denaturation. Hybridization after the regeneration process on the surface of bioelectrode was performed for six consecutive measurements and resultant change in R_{ct} value was recorded (Fig. S8(B)). The ΔR_{ct} value of the bioelectrode was found to decrease after each regeneration cycle and a reduction to about 89% of initial value after sixth cycle was observed. Although, a slight increase in the R_{ct} value for pDNA/t-PANI-NT/ITO bioelectrode after each regeneration cycle and decrease in the R_{ct} value after the hybridization indicates the incomplete denaturation and nonspecific adsorption of the target DNA on the surface of bioelectrode during the process. For determining the reproducibility of the fabricated pDNA/t-PANI-NT/ITO and pDNA/c-PANI-NT/ITO bioelectrodes, the relative standard deviation (RSD) was calculated. For RSD calculation two different concentrations of the cDNA (10^{-15} M and 10^{-11} M) were immobilized on five equally prepared bioelectrodes and their R_{ct} value was calculated. For pDNA/t-PANI-NT/ITO bioelectrode the values of RSD were found to be 5.7% and 4.8% for 10^{-15} M and 10^{-12} M concentration of cDNA, respectively and for pDNA/c-PANI-NT/ITO bioelectrode the values of RSD were found to be 7.6% and 6.4% for 10^{-15} M and 10^{-11} M concentration of cDNA respectively. The low RSD value for pDNA/t-PANI-NT/ITO bioelectrode in comparison to the pDNA/c-PANI-NT/ITO bioelectrode suggested the better repeatability of the proposed biosensor.

Further, the storage stability of the fabricated pDNA/t-PANI-NT/ITO and pDNA/c-PANI-NT/ITO bioelectrodes was investigated *via* EIS by recording five measurements each week for 40 days [42]. It was observed that the decrease in the signal response to 5% of its original R_{ct} value was found after 20days for pDNA/t-PANI-NT/ITO bioelectrode (Fig. 7(D); curve (i)) and 15days for pDNA/c-PANI-NT/ITO bioelectrode (Fig. 7(D); curve (ii)), when the electrode was stored in the refrigerator at 4 °C.

4. Conclusions

In summary, we have synthesized PANI-NT by using MnO_2 as a sacrificial template. The t-PANI NT were successfully electrophoretically deposited on ITO coated glass substrates. The morphological and electrochemical studies clearly reveal that the t-PANI NT have conducive morphology, improved conductivity, and better redox activity compared to PANI-MnO_2 NT and c-PANI-NT. Further t-PANI-NT/ITO electrodes were utilized as an impedimetric nucleic acid sensor for specific detection of CML. The fabricated genosensor was found to detect a wide range of complementary DNA concentration (10^{-6} to 10^{-16} M) with lower detection limit (10^{-16} M), good reproducibility and high stability (40 days). The biosensor was able to distinguish the clinical samples of CML positive and negative patients. Besides this, attempts are being made for the construction of highly sensitive genosensor with a wide variety of nucleic acid detection applications that may have importance in point-of-care diagnostics.

Acknowledgements

We thank Director, National Physical Laboratory, India for providing facilities. A.S. is thankful to CSIR, India, for the award of SRF. C.M. P. acknowledges the financial support received from Department of Science and Technology, India under DST-INSPIRE Faculty Project (Grant No. DST/INSPIRE/04/2015/000932). S.S. is grateful to UGC, India for the award of SRF. We thank Prof. B.D Malhotra (Delhi Technological University, Delhi, India) for useful discussions. Author thanks, Dr. Birendra Kumar Yadav (Rajiv Gandhi Cancer Institute and Research Centre, New Delhi) for providing the clinical patient samples.

Appendix A. Supplementary material

Supplementary data associated with this article can be found in the online version at http://dx.doi.org/10.1016/j.talanta.2018.05.038.

References

[1] D. Li, J. Huang, R.B. Kaner, Acc. Chem. Res. 42 (2008) 135–145.
[2] G.-R. Li, Z.-P. Feng, J.-H. Zhong, Z.-L. Wang, Y.-X. Tong, Macromolecules 43 (2010) 2178–2183.
[3] H.-W. Park, T. Kim, J. Huh, M. Kang, J.E. Lee, H. Yoon, ACS Nano 6 (2012) 7624–7633.
[4] W. Chen, R.B. Rakhi, H.N. Alshareef, J. Mater. Chem. A 1 (2013) 3315–3324.
[5] X. Feng, Y. Zhang, Z. Yan, N. Chen, Y. Ma, X. Liu, X. Yang, W. Hou, J. Mater. Chem. A 1 (2013) 9775–9780.
[6] V. Talwar, O. Singh, R.C. Singh, Sens. Actuators B: Chem. 191 (2014) 276–282.
[7] X. Shi, A.L. Briseno, R.J. Sanedrin, F. Zhou, Macromolecules 36 (2003) 4093–4098.
[8] Z. Zhang, J. Sui, L. Zhang, M. Wan, Y. Wei, L. Yu, Adv. Mater. 17 (2005) 2854–2857.
[9] L. Xia, Z. Wei, M. Wan, J. Colloid Interface Sci. 341 (2010) 1–11.
[10] L. Pan, H. Qiu, C. Dou, Y. Li, L. Pu, J. Xu, Y. Shi, Int. J. Mol. Sci. 11 (2010) 2636–2657.
[11] W. Chen, R.B. Rakhi, H.N. Alshareef, J. Mater. Chem. C 117 (2013) 15009–15019.
[12] I. Tiwari, M. Gupta, C.M. Pandey, V. Mishra, Dalton Trans. 44 (2015) 15557–15566.
[13] C. Dhand, M. Das, G. Sumana, A.K. Srivastava, M.K. Pandey, C.G. Kim, M. Datta, B.D. Malhotra, Nanoscale 2 (2010) 747–754.
[14] Y. Zhu, J. Zhang, Y. Zheng, Z. Huang, L. Feng, L. Jiang, Adv. Funct. Mater. 16 (2006) 568–574.
[15] L. Li, Y. Shi, L. Pan, Y. Shi, G. Yu, J. Mater. Chem. B 3 (2015) 2920.
[16] C. Dhand, M. Das, M. Datta, B.D. Malhotra, Biosens. Bioelectron. 26 (2011) 2811–2821.
[17] T. Sen, S. Mishra, N.G. Shimpi, RSC Adv. 6 (2016) 42196–42222.
[18] Y.-Z. Long, M.-M. Li, C. Gu, M. Wan, J.-L. Duvail, Z. Liu, Z. Fan, Prog. Polym. Sci. 36 (2011) 1415–1442.
[19] R. Liu, S.B. Lee, J. Am. Chem. Soc. 130 (2008) 2942–2943.
[20] M. Yang, J. Ma, C. Zhang, Z. Yang, Y. Lu, Angew. Chem. Int. Ed. 44 (2005) 6727–6730.
[21] M.W.N. Deininger, J.M. Goldman, J.V. Melo, Blood 96 (2000) 3343–3356.
[22] J.P. Radich, T. Gooley, E. Bryant, T. Chauncey, R. Clift, L. Beppu, S. Edmands, M.E.D. Flowers, K. Kerkof, R. Nelson, Blood 98 (2001) 1701–1707.
[23] J. Chen, J. Zhang, L. Huang, X. Lin, G. Chen, Biosens. Bioelectron. 24 (2008) 349–355.
[24] A.S. Advani, A.M. Pendergast, Leuk. Res. 26 (2002) 713–720.
[25] A.S. Corbin, A. Agarwal, M. Loriaux, J. Cortes, M.W. Deininger, B.J. Druker, J. Clin. Investig. 121 (2011) 396.
[26] M.A. Tainsky, Biochim. Biophys. Acta 1796 (2009) 176–193.
[27] M. Shamsipur, V. Nasirian, A. Barati, K. Mansouri, A. Vaisi-Raygani, S. Kashanian, Anal. Chim. Acta 966 (2017) 62–70.
[28] D. Ozkan-Ariksoysal, Y.U. Kayran, F.F. Yilmaz, A.A. Ciucu, I.G. David, V. David, M. Hosgor-Limoncu, M. Ozsoz, Talanta 166 (2017) 27–35.
[29] T. Yu, H. Zhang, Z. Huang, Z. Luo, N. Huang, S. Ding, W. Feng, Electroanalysis 29 (2017) 828–834.
[30] Y.-X. Chen, K.-J. Huang, F. Lin, L.-X. Fang, Talanta 175 (2017) 168–176.
[31] C.M. Pandey, G. Sumana, K.N. Sood, B.D. Malhotra, Thin Solid Films 519 (2010) 1178–1183.
[32] A.S. Ghrera, C.M. Pandey, B.D. Malhotra, Sens. Actuators B: Chem. 266 (2018) 329–336.
[33] K.Y.P.S. Avelino, I.A.M. Frias, N. Lucena-Silva, R.G. Gomes, C.P. de Melo, M.D.L. Oliveira, C.s.A.S. Andrade, Colloids Surf. B 148 (2016) 576–584.
[34] R. Singh, R. Verma, G. Sumana, A.K. Srivastava, S. Sood, R.K. Gupta, B.D. Malhotra, Bioelectrochemistry 86 (2012) 30–37.
[35] N. Hui, X. Sun, S. Niu, X. Luo, ACS Appl. Mater. Interfaces 9 (2017) 2914–2923.
[36] C. Dhand, P.R. Solanki, M.K. Pandey, M. Datta, B.D. Malhotra, Electrophoresis 31 (2010) 3754–3762.
[37] L. Zhang, M. Wan, Nanotechnology 13 (2002) 750.
[38] R. Singh, R. Prasad, G. Sumana, K. Arora, S. Sood, R.K. Gupta, B.D. Malhotra, Biosens. Bioelectron. 24 (2009) 2232–2238.
[39] A. Sumboja, C.Y. Foo, J. Yan, C. Yan, R.K. Gupta, P.S. Lee, J. Mater. Chem. 22 (2012) 23921–23928.
[40] J. Stejskal, J. Prokes, M. Trchovs, Polym. Degrad. Stab. 102 (2014) 67–73.
[41] S. Solanki, C.M. Pandey, A. Soni, G. Sumana, A.M. Biradar, Microchim. Acta 183 (2015) 167–176.
[42] A. Soni, C.M. Pandey, S. Solanki, G. Sumana, RSC Adv. 5 (2015) 45767–45774.
[43] B.G. Choi, H. Park, M.H. Yang, Y.M. Jung, S.Y. Lee, W.H. Hong, T.J. Park, Nanoscale 2 (2010) 2692–2697.
[44] M.U.A. Prathap, R. Srivastava, B. Satpati, Electrochim. Acta 114 (2013) 285–295.
[45] Y. Bo, H. Yang, Y. Hu, T. Yao, S. Huang, Electrochim. Acta 56 (2011) 2676–2681.
[46] H.-L. Shuai, K.-J. Huang, Y.-X. Chen, J. Mater. Chem. B 4 (2016) 1186–1196.
[47] C.M. Pandey, I. Tiwari, G. Sumana, RSC Adv. 4 (2014) 31047–31055.
[48] N. Prabhakar, H. Singh, B.D. Malhotra, Electrochem. Commun. 10 (2008) 821–826.
[49] Y. Hao, B. Zhou, F. Wang, J. Li, L. Deng, Y.-N. Liu, Biosens. Bioelectron. 52 (2014) 422–426.
[50] Q. Zhu, F. Gao, Y. Yang, B. Zhang, W. Wang, Z. Hu, Q. Wang, Sens. Actuators B: Chem. 207 (2015) 819–826.
[51] J. Wilson, S. Radhakrishnan, C. Sumathi, V. Dharuman, Sens. Actuators B: Chem. 171 (2012) 216–222.
[52] Q. Zheng, H. Wu, Z. Shen, W. Gao, Y. Yu, Y. Ma, W. Guang, Q. Guo, R. Yan, J. Wang, Analyst 140 (2015) 6660–6670.